

Three Emission-Line Galaxies at $z \sim 2.4$

Richard Meyer¹

California Polytechnic University, San Luis Obispo, CA

`rmeyer@calpoly.edu`

David Thompson

California Institute of Technology, Pasadena, CA

`djt@iraastro.caltech.edu`

and

Filippo Mannucci

C.A.I.S.M.I.—C.N.R., Florence, Italy

`filippo@arcetri.astro.it`

ABSTRACT

We present Keck near-infrared and WIYN optical photometry of a sample of galaxies detected by near-infrared narrowband imaging in the fields of quasar metal absorption line systems at $z \sim 2.4$. Wide separations ($0.6\text{--}1.6 h^{-1}$ Mpc) from the quasars indicates that they are not directly responsible for the absorption systems. From the color excess of the galaxies we derived line fluxes, star formation rates, and equivalent widths. The data are consistent with one source having an active nucleus and two sources containing regions of star formation. The blue (R-K) colors for the sources suggest relatively lesser dust content. We discuss possible projects using current wide-field infrared instruments, which can cover an order of magnitude greater area with modest allocations of telescope time.

Subject headings: emission-line galaxies

1. Introduction

A complete understanding of the physical processes involved in the formation of galaxies requires a knowledge of the young galaxy populations at high redshift. These primeval galaxies are thought to exhibit bursts of star formation possibly associated with active galactic nuclei (AGNs), detectable through the resulting strong emission lines. Various detection techniques have been explored over the years in search of these star forming galaxies. Each detection technique introduced has both advantages and disadvantages,

and therefore it is important to explore many different techniques to obtain a view of the primeval galaxy population as complete as possible.

The Lyman-alpha emission line has been the target of many surveys aimed at the detection of high redshift galaxies (see reviews by Pritchett (1994); Thommes et. al. (1998)), but turned up only a small fraction of the expected number of strong emission line sources. More recent deep surveys (Cowie & Hu 1998; Hu et. al. 1998, 1999; Pascarella et. al. 1998; Kudritzki et. al. 2000) have detected some Ly α emitters, but at lower luminosity. The Large-Area Lyman Alpha survey (Rhoads et. al. 2001) currently being conducted has turned up a number of Ly α emitters, indicating that these

¹Summer Undergraduate Research Fellow, California Institute of Technology, Pasadena, CA

sources are detectable with an adequate volume coverage and sensitivity.

An alternative method, which does not rely on the presence of a strong Ly α line, is the Lyman Break technique (Steidel & Hamilton 1992, 1993; Steidel et. al. 1995). This technique involves the detection of both a blue UV continuum and the Lyman limit spectral drop at a rest-frame 912 Å. This technique has proved very effective at identifying $3 \leq z \leq 3.5$ galaxies. Spectroscopic analysis (Steidel et. al. 1996) has shown a near zero mean Ly α emission, which is consistent with the lack of strong Ly α emitters in the line-based surveys. Highly reddened sources would not be selected by the Lyman Break technique.

High redshift ($z \geq 1$) near-infrared emission-line surveys search for rest-frame optical emission lines, such as H α λ 6563, [O III] λ 5007, H β λ 4861, or [O II] λ 3727. The attenuating effects of dust are far less at longer wavelengths, so these emission lines can be detectable in dustier galaxies. Ground-based emission line surveys have primarily targeted fields containing objects with known redshifts ($z > 2$), typically quasars and radio galaxies (Bunker et. al. 1995; Pahre & Djorgovski 1995; Thompson et. al. 1996), or damped Ly α systems and strong metal absorbers, (Tepliz et. al. 1998; Mannucci et. al. 1998), but also blank fields (Moorwood et. al. 2000). In addition, McCarthy et. al. (1999) used the Hubble Space Telescope NICMOS camera to conduct a parallel, slitless spectroscopic survey. Targets are selected at specific redshifts which place the strong optical lines into the bandpasses of existing near-infrared narrowband filters. Malkan et. al. (1995) and Beckwith et. al. (1998) spectroscopically confirmed two emission-line galaxies.

In this paper we present followup observations on the 18 candidate emission-line objects from Mannucci et. al. (1998, hereafter MTBW98), identified in a survey covering 227 arcmin². We obtained both optical and near-infrared observations on the majority of their sources. Our goal was to investigate the morphology, color, and confirm the presence of the emission lines. In §2 we describe the observations and reduction methods. In §3 we discuss the results, including possible reasons for why many of the objects were not confirmed. Finally, in §4 we summarize our results and discuss prospects for future surveys using a narrowband

near-infrared imaging technique. For simplicity and to ease comparisons with prior surveys, we assume a cosmology of $H_0 = 100 h \text{ km s}^{-1} \text{ Mpc}^{-1}$, $\Omega_M = 1$ and $\Omega_\Lambda = 0$. Assuming a Lambda cosmology, with $H_0 = 70 \text{ km s}^{-1} \text{ Mpc}^{-1}$, $\Omega_M = 0.3$ and $\Omega_\Lambda = 0.7$, would increase projected separations by a factor of two, or the derived star formation rates or areas surveyed by a factor of four.

2. Observations & Reductions

2.1. Optical Imaging

Deep R band images covering 12 of the 18 emission-line candidates from MTBW98 were acquired with the CCD imager in the queue observing mode of the 3.5m WIYN telescope from August to November 1997. The imager uses a 2048² pixel CCD at 0".195 per 21 μ m pixel, resulting in a 6'.66 square field of view. The data were obtained using a Harris R filter with a central wavelength of 646nm and a full width at half maximum (FWHM) of 153nm.

Standard CCD processing was used to bias-subtract, flatfield, mask the hot pixels, align, and then stack the images. The seeing in the data were good, with an average 0".62 FWHM.

The deep observations were not obtained under photometric conditions, so calibration images were acquired for each field during photometric weather on subsequent nights. The photometric images were calibrated onto the Vega scale using the Landolt (1992) standards. The images reach limiting (5σ) magnitudes between 25^m.7 and 26^m.4.

2.2. Infrared Imaging

Infrared images were taken in either the J or K band, and in the corresponding 1.237 μ m or 2.248 μ m narrowband (NB, $\delta\lambda/\lambda \sim 0.01$) filters for 15 of the 18 sources from MTBW98. Images were obtained on UT 1999 July 22 and 23 with the Near-Infrared Camera (NIRC; Matthews & Soifer 1994) on the Keck I telescope. NIRC uses a 256² InSb detector at 0".15 pixel⁻¹ resulting in 38".4 square field of view. The data consisted of 10-15 dithered images for each object, with 30s exposures for the broadband (BB) data and 180s for the narrowband data. Thus, typical exposure times were 5 minutes in the broadband filters and 30 minutes in the narrowband filters. The seeing

ranged from $0''.3$ to $0''.5$ FWHM in K and $0''.5$ to $0''.6$ in J . All observations were obtained under photometric conditions.

Using IRAF² routines, images were dark subtracted and flatfielded using a combination of domeflats and skyflats. The bad pixels were masked using separate narrowband and broadband bad pixel masks because the longer exposure times for the narrowband images resulted in more saturated hot pixels. Images were then aligned and stacked.

The broadband data were calibrated onto the Vega scale using the Persson et. al. (1998) standard stars. The narrowband zero-points were scaled to the broadband data to give the continuum objects in a given filter set a zero mean color for the night. Photometry on the objects was extracted in a $2''$ diameter aperture. This relatively small aperture was used to minimize contamination from nearby objects. The photometric uncertainties quoted in Table 1 are determined by the IRAF/apphot package from a local measure of the sky noise around each source. The uncertainties are not corrected for errors in determining the zero points, which we estimate at 3% for the broadband data and 10% for the narrowband data. This has no effect on the relative colors of the sources.

3. Results & Discussion

We constructed color magnitude diagrams for each field, plotting the (BB-NB) color against the narrowband magnitude. Continuum objects appear at zero color because of the relative photometric calibration of the narrowband images. An emission-line object will have a positive color since the total flux of the narrowband image will be due mostly to the emission-line and not the continuum.

In addition, the broadband and narrowband image pairs were “blinked” in order to visually confirm the sources with excess narrowband flux as well as search for new emission line galaxies. The images were displayed such that the continuum objects in the field had the same apparent brightness in both images, thus emission-line sources appear brighter in the narrowband image relative to the

broadband. Of the fifteen emission-line candidates from MTBW98 we confirmed strong emission in three sources, with (BB-NB) colors ranging from 0.75 to 2.22 magnitudes. No new emission-line sources were identified.

In the following sections we present notes on the individual sources. Table 1 lists the optical and near-infrared magnitudes and uncertainties for each source, as well as values derived from the color excess, such as the line equivalent widths, line fluxes, and star formation rates (SFR). Figures 1-3 show broadband and narrowband image pairs for each confirmed emission-line source and a color magnitude diagram. The color magnitude diagrams were plotted from larger images ($\sim 60''$ square), and therefore contain data for more sources than are visible in the $20''$ square images.

3.1. Q0100+13B

The field of quasar Q0100+130 (PHL 957) was targeted by MTBW98 due to the presence of a strong C IV absorption line system at $z = 2.308$ (York et. al. 1991), which places the redshifted [O II] $\lambda 3727$ line at $1.237\mu\text{m}$. The emission line candidate Q0100+13B shows a strong emission-line with a (J- $1.237\mu\text{m}$) color excess of 1.04 ± 0.20 magnitudes. We derived a rest frame equivalent width of 60\AA and a line flux of 1.61×10^{-16} ergs $\text{cm}^{-2} \text{s}^{-1}$. Assuming the emission-line is [O II] $\lambda 3727$ at $z = 2.31$, we used an [O II] to H α line ratio in Kennicutt (1992) with no correction for extinction to derive a star formation rate of $31 h^{-2} M_{\odot} \text{yr}^{-1}$. If significant dust extinction is present, this star formation rate is a lower limit.

Q0100+13B is separated from the quasar by $51''.2$ at a position angle (PA) of $35^{\circ}.6$. The corresponding projected comoving separation from the quasar is $668 h^{-1} \text{kpc}$ ($202 h^{-1} \text{kpc}$ proper separation). This is much larger than the size of an individual galaxy. Since this source has the lowest projected separation of the three confirmed emission-line objects from their corresponding quasar’s line-of-sight, none of these galaxies are likely to be responsible for the absorption-line systems targeted by MTBW98.

Q0100+13B is marginally resolved with a $0''.6$ FWHM in the continuum subtracted image, however there are no good point sources in the NIRC

²IRAF is distributed by the National Optical Astronomy Observatories, which are operated by the Association of Universities for Research in Astronomy, Inc., under cooperative agreement with the National Science Foundation.

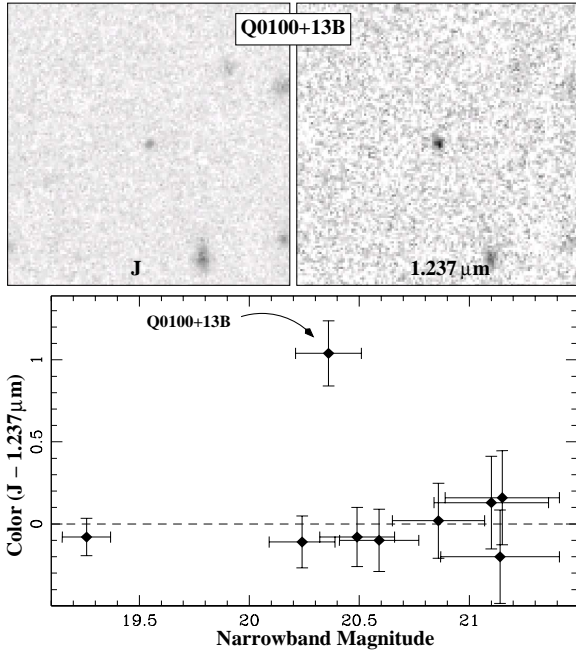


Fig. 1.— Top: J band (left) and $1.237\mu\text{m}$ narrowband (right) NIRC images of Q0100+13B (centered in both images). The J band image has been scaled so that the continuum objects appear the same in both images. Images are $20''$ square, with north up and east to the left. Bottom: color magnitude diagram of the full $60''$ field around Q0100+13B.

image to directly compare to and we used a seeing average of $0''.5$ FWHM for the night in the J filter. The moderate equivalent width and the slightly resolved morphology make Q0100+13B more consistent with the interpretation that the line emission is powered star formation, but with the current data we can not rule out an active nucleus.

3.2. Q0201+36D

The quasar Q0201+365 was targeted because of a strong C IV absorption line system at $z=2.424$ (Sargent et. al. 1989; York et. al. 1991), which places the redshifted $H\alpha$ at $2.248\mu\text{m}$. We confirm strong emission from the candidate Q0201+36D, with a $(K-2.248\mu\text{m})$ color excess of 0.75 ± 0.19 magnitudes. We derived a rest frame equivalent width of 67 \AA and a line flux of $1.29 \times 10^{-16} \text{ ergs cm}^{-2} \text{ s}^{-1}$. Assuming the line is $H\alpha$ at $z = 2.42$, we used the luminosity to $H\alpha$ ratio from Kennicutt (1992) to derive a SFR of $12 h^{-2} M_{\odot} \text{ yr}^{-1}$. Q0201+36D is separated from the quasar by $116''.3$ at $\text{PA}=141^{\circ}1$.

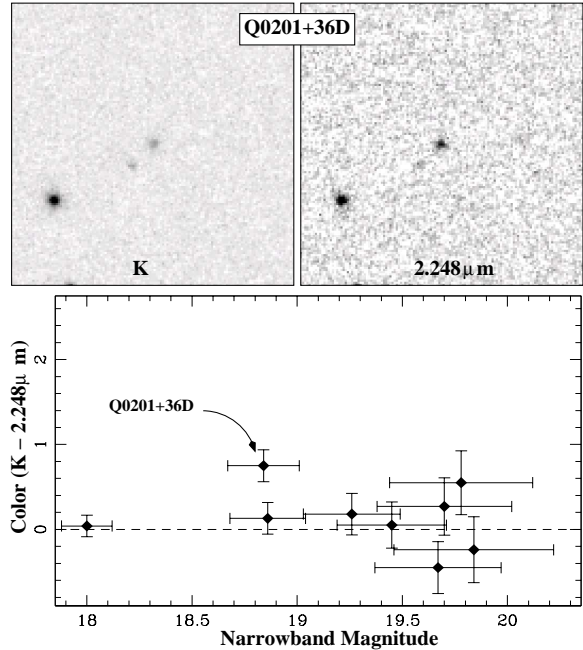


Fig. 2.— As in Fig. 1, K band and $2.248\mu\text{m}$ narrowband images with color magnitude diagram of the field.

The corresponding projected comoving separation is $1.55 h^{-1} \text{ Mpc}$.

The seeing in the Q0201+36D field was $0''.4$ FWHM. A profile fit to the continuum subtracted image failed to converge, so we resorted to a more subjective assessment of the source resolution. A bright point source was extracted from elsewhere in the image, scaled down to a comparable flux as the emission line source, and then shifted and added back into the image next to the emission line source. A visual comparison of the two shows that Q0201+36D is clearly resolved. If the emission is $H\alpha$ at a redshift 2.42, then the relatively low equivalent width and star formation rate, along with the diffuse nature of the emission line flux, suggest that this source is a star forming galaxy and not an AGN.

3.3. Q2038-01D

As with the other two sources, the quasar Q2038-012 was targeted due to a strong C IV absorption line at $z=2.424$ (Sargent et. al. 1989; York et. al. 1991). We confirm strong emission in candidate Q2038-01D in the $2.248\mu\text{m}$ nar-

rowband filter. Our data show that Q2038-01D is resolved into two compact sources, both with emission lines, separated by $0''.8$ ($10 h^{-1}$ kpc). By masking out one source and measuring the photometry on the other, we measured the north-east (NE) and south-west components to have a color excess of 1.91 ± 0.41 and 2.88 ± 0.46 magnitudes, respectively. The derived rest-frame equivalent widths are quite high, over 10^4 \AA for the SW component under the assumption that the line is $H\alpha$ at the targeted redshift. Such a high equivalent width would be unusual even for an active nucleus. There remains the possibility that this source is at a higher redshift, perhaps seen in the [O III] or [O II] line. Spectroscopic data covering one or more additional lines could resolve this issue. We note that the equivalent width becomes highly non-linear for a $(K - 2.248\mu\text{m})$ color in excess of two magnitudes, going to infinity at $2^{\text{m}}96$ where all of the broadband flux is from the emission line. Q2038-01D is $120''.8$ from the quasar at PA= $126^\circ5$. The corresponding projected comoving separation is $1.60 h^{-1}$ Mpc.

The seeing in these data were especially good with an average of $0''.3$ FWHM. We measured the FWHM of each object by first masking out the other source. Both components were formally resolved, with a $0''.45$ FWHM, but the SW component appears more compact. Faint, diffuse, elongated emission is visible on both sides of these sources in the narrowband image.

Q2038-01D is most likely two galaxies in the process of merging, where the gravitational interaction is fueling perhaps both star formation and an AGN. While the rest-frame equivalent width in the NE component is possible to produce with a pure starburst, the much larger equivalent width in the SW component almost surely indicates the presence of an active nucleus.

3.4. Source Colors

All three confirmed emission-line objects had bluer (R-K) colors than the unconfirmed objects from MTBW98. The (R-K) colors³ for the three confirmed sources range from 2.97 to 3.28 magnitudes. The mean color for a field sample at similar K-band magnitudes is 3.93 (Thompson et. al.

³We converted Q0100+13B's R-J color of 2.2 to R-K assuming a J-K of 1.

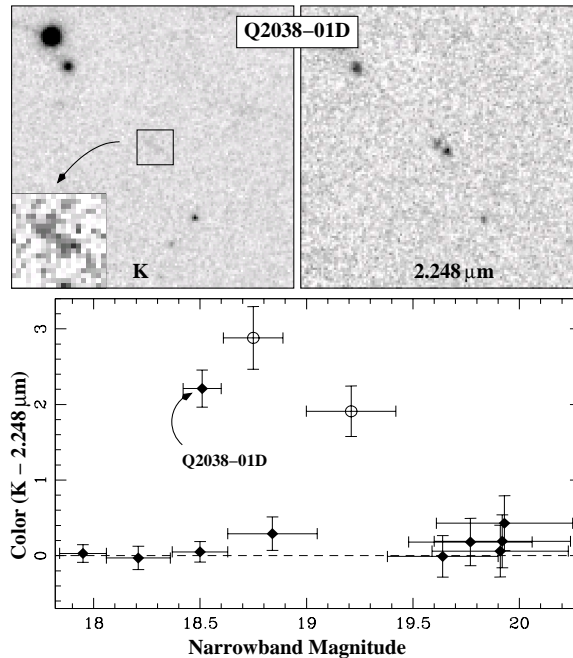


Fig. 3.— As in Fig. 1, K band and $2.248\mu\text{m}$ narrowband images for Q2038-01D, with a color magnitude diagram for the full field. The open circles mark the photometry derived separately for the two components. The inset shows in more detail the $3''$ box around the K -band image of Q2038-01D.

1999), indicating that these emission-line objects may not suffer from heavy dust obscuration, and it would be interesting to see if the rest-frame UV lines are visible with visual wavelength spectroscopy. While the original survey (MTBW98) should be sensitive to emission-line sources with more dust extinction than the UV techniques, in practice any objects with emission lines in the narrowband filter would be identified. This may indicate that very dusty sources are rare, but the number of objects found is still small.

3.5. Unconfirmed Sources

Twelve of the fifteen candidates from MTBW98 did not show signs of an emission-line in our data. We propose two possibilities to explain this. The most straightforward scenario is that the objects are not truly emission-line sources, but spurious detections in the narrowband survey data. The other scenario is that instrumental idiosyncrasies could combine to cause effective shifts between the

actual band-passes of the narrowband filters.

Each candidate object in MTBW98 was given a rank degree of significance, with 1 as the highest and 3 as the lowest. All three of our confirmed sources had a rank of 1 or 2, while the unconfirmed candidates had ranks of 2 or 3. Each of our confirmed objects has the highest signal to noise ratio (SNR) of all objects in the same field, ranging from 3.0 to 5.6σ in MTBW99, and the SNR was very low for many of the other sources. So perhaps the emission-line candidates are simply spurious detections, selected from noise peaks in the narrowband survey data. We consider this the most likely explanation.

The other possibility for a lack of emission-line detection is due to effective bandpass shifts between the narrowband filters used in the survey and this followup. The actual bandpass of the narrowband filters, as seen by individual objects, is a function of both its relative position in the field and any tilts of the filters in the pupil planes of either instrument. These effects are difficult to quantify a posteriori. By using two separate filters with these unknown variables, an emission line may be within the bandpass of one filter, but not necessarily the other. Therefore we cannot conclusively rule out the presence of emission lines in our twelve unconfirmed sources.

4. Summary

We observed 15 candidate emission-line sources from MTBW98 and confirmed strong emission in three. These galaxies may be associated with quasar metal absorption line systems at $z \sim 2.4$, however, wide separations ($0.6\text{-}1.6 h^{-1}$ Mpc) from the quasars indicates that they are not directly responsible for the absorption systems. While it is likely these galaxies are at the targeted redshifts, confirmation requires spectroscopic observations of one or more additional emission lines. From the color excess of the galaxies we derived line fluxes, star formation rates, and equivalent widths. Source resolution and line equivalent widths in two galaxies are consistent with line emission powered by star formation, while the third galaxy, which is actually double, is consistent with the presence of an active nucleus. The blue (R-K) colors for the sources, as compared to field galaxies, suggest a relatively low dust content. These galaxies may

therefore be detectable in Ly α or other rest-frame UV emission lines.

4.1. Future Prospects

A new generation of near-infrared instruments with larger fields of view are now available. Here we examine the feasibility of conducting new narrowband infrared surveys.

Several new, wide-field near-infrared instruments are currently working or nearing completion on 4m class telescopes. Here we specifically consider Omega-2000 (Bailer-Jones et. al. 2000) at the Calar Alto 3.5 m telescope, with a 15.4×15.4 arcmin² field of view, WIRC-2k (Wilson et. al. 2002) at the Palomar 200-inch telescope with a 8.3×8.3 arcmin² field of view, and FLAMINGOS (Elston 1998) at the Kitt Peak 4 m telescope with a 10×10 arcmin² field of view. MTBW98 reached line flux limits of $\sim 2 \times 10^{-16}$ ergs cm⁻² s⁻¹, which we consider to be a conservative estimate for the new cameras, assuming 2 hour narrowband plus 30 minute broadband exposure times. Under these assumptions, new narrowband surveys can cover an order of magnitude more area than MTBW98 in just 3-10 nights, a moderate-sized project, especially when split over more than one semester. Note that the large fields of view cover projected comoving fields of up to $12 \times 12 h^{-2}$ Mpc² at $z=2.4$, much larger than the size of a cluster core. Even surveys targeting known objects would then largely sample blank fields. Removing the restriction of where to point, a purely blank field survey is free to target regions with low Galactic dust extinction and use the narrowband filters with maximum transmission or minimum background to increase the survey depth. Additional survey volume can be covered at the expense of reducing the color contrast by using somewhat broader narrowband filters (e.g. $\delta\lambda/\lambda \sim 2 - 3\%$).

For 8 m-class telescopes, currently operating near-infrared instruments include ISAAC on the ESO VLT UT1 (Moorwood 1997), with a field of view of 2.5×2.5 arcmin², CISCO on the Subaru telescope, with a field of view 1.8×2.5 arcmin² (Motohara et al. 2002), and NIRI on the Gemini-North telescope (Hora et. al. 1995), with a 2×2 arcmin² field of view. Under the same assumptions as before, an order of magnitude more area than Tepliz et. al. (1998) can be covered to similar depth in 6-10 nights. The fields of view are

comparable to the MTBW98 survey, $\sim 2 h^{-1}$ Mpc, and thus it may be preferable to continue targeting known high-redshift sources. In the years since the MTBW98 or Teplitz et. al. (1998) surveys were done, many new quasar damped Ly α and metal absorption line systems have been discovered, significantly increasing the list of potential targets.

We would like to thank Dr. B.T. Soifer for the funding that made this Summer Undergraduate Research Fellowship (Caltech SURF project) possible.

REFERENCES

- Bailer-Jones, C., Bizenberger, P., Storz, C. 2000, Proc. SPIE, 4008, 1305
- Beckwith, S.V.W., Thompson, D., Mannucci, F., & Djorgovski, S.G. 1998 ApJ, 504, 107
- Bunker, A.J., Warren, S.J., Hewitt, P.C., & Clements, D.L. 1995, MNRAS, 273, 513
- Cowie, L.L., & Hu, E.M. 1998, AJ, 115, 1319
- De Propriis, R., Pritchet, C. J., Hartwick, F. D. A., & Hickson, P. 1993, AJ, 105, 1243
- Elston, R. 1998, Proc. SPIE, 3354, 404
- Francis, P., Woodgate, B., Stephen, W., Møller, P., Mazzolini, M., Bunker, A., Lowenthal, J., Williams, T., Minezaki, T., Kobayashi, Y., & Yoshii, Y. 1996, ApJ, 457, 490
- Hora, J. L., Hodapp, K-W., Irwin, E. M., Keller, T. J., Young, T. T. 1995, Proc. SPIE, 2475, 308
- Hu, E.M., Cowie, L.L., & McMahan, R.G. 1998, ApJ, 502, L99
- Hu, E.M., McMahan, R.G., & Cowie, L.L. 1999, ApJ, 522, L9
- Kennicutt, R.C., Jr. 1983, ApJ, 272, 54
- Kennicutt, R.C., Jr. 1992, ApJ, 388, 310
- Kudritzki, R.-P.; Méndez, R. H., Feldmeier, J. J., Ciardullo, R., Jacoby, G. H., Freeman, K. C., Arnaboldi, M., Capaccioli, M., Gerhard, O., & Ford, H. C. 2000, ApJ, 536, 19
- Landolt, A. 1992. AJ, 104, 340.
- Malkan, M., Teplitz, & H., McLean, I. 1995, ApJ, 448, L5
- Mannucci, F. & Beckwith, S.V.W. 1995. ApJ, 442, 569
- Mannucci, F., Thompson, D., Beckwith, S .V. W., & Williger, G. M. 1998, ApJ, 501, 11
- Matthews, K., & Soifer, B. T. 1994, in Infrared Astronomy with Arrays: the Next Generation, ed. I. McLean (Dordrecht: Kluwer Academic Publishers), 239
- McCarthy, P.J., Yan, L., Freudling, W., Teplitz, H.I., Malumuth, E.M., Weymann, R.J., Malkan, M.A., Fosbury, R.A.E., Gardner, J.P., Storrie-Lombardi, L.J., Thompson, R.I., Williams, R.E., Heap, S.R. 1999. ApJ, 520, 548
- Moorwood, A. F. 1997, Proc. SPIE, 2871, 1146
- Moorwood, A.F.W., van der Werf, P.P., Cuby, J.G., & Oliva, E. 2000, A&A, 362, 9
- Motohara, K., Iwamuro, F., Maihara, T., Oya, S., Tsukamoto, H., Imanishi, M., Terada, H., Goto, M., Iwai, J., Tanabe, H., Hata, R., Taguchi, T., & Harashima, T. 2002, PASJ, 54, 315
- Pascarelle, S.M., Windhorst, R.A. & Keel, W.C. 1998, AJ, 116, 2659
- Pahre, M.A., & Djorgovski, S.G. 1995, ApJ, 449, L1
- Parkes, I., Collins, C.A., & Joesph, R.D. 1994, MNRAS, 268, 983
- Persson, S. E., Murphy, D. E., Krzeminski, W., Roth, M., & Rieke, M. J. 1998, AJ, 116, 274
- Pritchet, C.J. 1994, PASP, 106, 1052
- Rhoads, J., Malhotra, S., Dey, A., Stern D., Spinrad, H., & Jannuzi, B. 2000, ApJ, 545, L85
- Sargent, W.L.W., & Steidel, C.C. 1989. ApJ, 69, 703
- Steidel, C. C., Giavalisco, M., Pettini, M., Dickinson, M., & Adelberger, K. L. 1996, ApJ462, 17
- Steidel, C.C., & Hamilton, D. 1992, AJ, 104, 941

- Steidel, C.C., & Hamilton, D. 1993, AJ, 105, 2017
- Steidel, C.C., Pettini, M., & Hamilton, D. 1995, AJ, 110, 2519
- Tepliz, H., Malkan, M., & McLean, I.S., 1998 ApJ, 506, 519.
- Thommes, E., Meisenheimer, K., Fockenbrock, R., Hippelein, H., Röser, H.-J., & Beckwith, S. 1998, MNRAS, 293, L6.
- Thompson, D. Beckwith, S.V.W., Fockenbrock, R. Fried, J., Hippelein, H., Huang, J.-S., von Kuhlmann, B., Leinert, Ch., Meisenheimer, K., Phleps, S., Röser, H.-J., Thommes, E., & Wolf, C. 1999, ApJ, 523, 100
- Thompson, D., & Djorgovski, S. 1995, AJ110, 982.
- Thompson, D., Mannucci F., & Beckwith S. V. W. 1996 AJ, 112 1794
- Van der Werf, P.P., 1997, Extragalactic Astronomy in the Infrared, ed. G.A. Mamon, Trinh Xuan Thuan and J. Tran Thanh Van, p. 451
- Wilson, J.C., Eikenberry, S.S., Henderson, C.P., Hayward, T.L., Carson, J.C., Pirger, B., Barry, D.J., Brandl, B., Houck, J.R., Fitzgerald, G.J., Stolberg, T.M. 2000, SPIE Proc. August 2002
- York, D., Yanny, B., Crotts, A., Carilli, C., & Garrison, E. 1991, MNRAS, 250, 24

TABLE 1
EMISSION-LINE OBJECTS

Object	Magnitudes ^a			Line Flux (ergs cm ⁻² s ⁻¹)	EQW _r ^b (Å)	SFR ^c (h ⁻² M _⊙ yr ⁻¹)
	BB _{IR}	NB _{IR}	R _{Harris}			
Q0100+13B	21.40±0.13	20.36±0.15	23.60±0.05	1.6 ± 0.3 × 10 ⁻¹⁶	60 ⁺²¹ ₋₁₇	31±6
Q0201+36D	19.59±0.08	18.84±0.17	22.87±0.03	1.3 ± 0.2 × 10 ⁻¹⁶	67 ⁺³¹ ₋₂₄	12±2
Q2038-01D	20.72±0.23	18.51±0.09	23.69±0.10	3.3 ± 0.3 × 10 ⁻¹⁶	835 ⁺⁵⁵¹ ₋₂₉₉	31±3
Q2038D-(NE)	21.12±0.26	19.21±0.21	...	1.6 ± 0.3 × 10 ⁻¹⁶	488 ⁺¹⁰⁰ ₋₂₅	15±3
Q2038D-(SW)	21.63±0.39	18.75±0.14	...	2.8 ± 0.4 × 10 ⁻¹⁶	> 11,000 ^d	26±4

^aQ0100+13B images taken using *J* and 1.237μm filters. Q0201+36D & Q2038-01D images taken using *K* and 2.248μm filters.

^bRest Frame Equivalent Width

^cStar Formation Rate

^dThe derived equivalent width is highly nonlinear at colors > 2 magnitudes, approaching infinity for (*K*-2.248μm) → 2^m96.